
Direct-Drive Fuel-Assembly Experiments with Gas-Filled, Cone-in-Shell, Fast-Ignition Targets on the OMEGA Laser

Introduction

The fast-ignition concept for inertial confinement fusion^{1,2} has the potential for higher gains and lower driver energies than central hot-spot ignition.³ The fast-ignition concept separates the fuel assembly and heating by using an ultrafast laser. The ultrafast laser produces relativistic electrons with high efficiency (up to 50% has been reported⁴) that heat the fuel, significantly easing the requirements on the compression driver.^{2,5} Laser or heavy-ion beam-heated hohlraums or direct-drive laser are options for the compression driver.

The biggest challenge of the fast-ignition concept is the transport of the relativistic electrons from the critical-density region ($n_e \sim 10^{21} \text{ cm}^{-3}$ for a typical 1- μm laser), where the ultrafast laser is absorbed and converted into electrons, to the compressed fuel—a distance that can be hundreds of microns in an ignition-scale target. For an electron beam divergence of $>20^\circ$, the overlap between the electron beam originating from a small focal spot ($\sim 10\text{-}\mu\text{m}$ radius) and the dense core with a diameter of $<50 \mu\text{m}$ would be very small.^{6,7} Most of the energy in the electron beam would be wasted. Two solutions have been proposed to minimize this standoff distance: a channeling beam to bore a hole in the plasma atmosphere around the core^{2,8} that allows the ultrafast laser to be absorbed closer to the core and a re-entrant cone to keep the path of the ultrafast laser free of plasma and bring it as close as possible to the dense core.^{9–11}

A few experiments have been performed to assess the potential of the re-entrant-cone concept. Integrated experiments at ILE-Osaka examined the coupling between the electron beam and the compressed core and found a 20%–30% energy transfer.^{11,12} A thousand-fold increase in neutron yield from 10^4 to 10^7 was observed by coupling a 0.5-PW, short-pulse laser into an empty CD target imploded by 2.5 kJ of laser light at a wavelength of 0.53 μm . A first series of hydro experiments¹³ with re-entrant cone targets in indirect-drive geometry on OMEGA studied the fuel assembly with 1 kJ of x-ray energy coupled to the capsule. Significant mixing between the gold cone and plastic shell material was observed. Mixing gold

into the dense fuel/shell material substantially increases the required ignition energy. Stephens *et al.* predicted that using direct drive would minimize the mixing between the gold cone and the fuel/shell material.¹³ Plasma filling the inside of the cone where the ultrafast laser has to propagate is another issue for cone targets. The high-pressure core plasma sends a shock wave through the gold cone that creates a plasma inside the cone when it breaks out, significantly increasing the electron propagation distance.

Fuel-assembly experiments with gas-filled, direct-drive, re-entrant cone-in-shell targets were performed on the OMEGA Laser System¹⁴ to study whether the cone-in-shell design is scalable to higher-energy densities and in preparation for future integrated experiments on the OMEGA EP laser,^{15,16} which will be operational in 2007. The experimental setup is described in the next section, which includes the laser configuration and imaging diagnostic arrangement. **Fuel Assembly in 35° and 70° Cone Targets** (p. 123) discusses backlighting of the fuel assembly of 35° and 70° cone targets. **Mixing of Au Cone and Core Material** (p. 124) reports an analysis of the mixing of cone and shell material, and **Compressed Core Areal Density Measurements** (p. 125) describes areal-density measurements using nuclear diagnostic methods. **Cone Filling** (p. 125) shows measurements of the shock breakout into the inside of the cone. Conclusions are presented in the last section, which also describes prospects for integrated experiments using the OMEGA EP laser.

Experimental Setup

Several different laser configurations were used for the direct-drive, cone-in-shell experiments on the 60-beam OMEGA laser. The targets were illuminated at a wavelength of 351 nm with a 1-ns square pulse and an energy of ~ 400 J per beam using two-dimensional smoothing by spectral dispersion (SSD)¹⁷ with 1-THz bandwidth in the UV and polarization smoothing (PS).¹⁸ The beams driving the shell used distributed phase plates (DPP).¹⁹ For the backlighting experiments, 15 beams ($\sim 6\text{-kJ}$ energy) were diverted to a backlighter foil of either vanadium (V) or iron (Fe) and focused to a spot size of

600 μm without DPP's. To provide a nearly uniform illumination of the shell, 15 beams were run at half energy and 20 beams at full energy, a total of ~ 11 kJ of laser energy driving the implosion. The nuclear diagnostics experiments used 55 beams, with ~ 21 kJ of total energy. The cone-filling experiments used 48 beams for the 70° cones or 54 beams for the 35° cones to avoid the laser hitting the inside of the cones.

The targets consist of gas-tight, $\sim 870\text{-}\mu\text{m}$ outer diameter, $24\text{-}\mu\text{m}$ -thick CH shells with a hollow gold cone with an opening angle of 35° or 70° inserted through a hole in the shell (see Fig. 103.6). The distance between the cone tip and the center of the shell, typically $30 \pm 10 \mu\text{m}$, is defined by a shelf on the cone that provides a gas-tight interface for the assembly. Both the 70° and 35° gold cones had a thickness of roughly $100 \mu\text{m}$ outside the shell, approximately $10 \mu\text{m}$ inside the shell, and end in a hyperbolic-shaped tip with its asymptotes intersecting $12 \mu\text{m}$ from the target center resulting in an Au thickness of $\sim 30 \mu\text{m}$ at the tip of the cone. Time-resolved x-ray framing cameras²⁰ recorded both backlit and self-emission images. The backlighter framing camera had an exposure time of ~ 40 ps and the self-emission camera ~ 80 ps. The framing cameras acquired 16 images with an ~ 60 ps temporal separation between exposures. Both cameras used a pinhole imager with a spatial resolution of $\sim 10 \mu\text{m}$ in the target plane. The self-emission camera was filtered with $\sim 200 \mu\text{m}$ of beryllium, with a lower cutoff at 50% transmission of ~ 3 keV. The backlighter camera used either a $25\text{-}\mu\text{m}$ -thick V filter to pass the predominantly He_α line

emission of the V backlighter at 4.95 keV or a $25\text{-}\mu\text{m}$ -thick Fe filter for the He_α line emission of a Fe backlighter at 6.7 keV. These filters suppress the thermal radiation from the implosion, improving the contrast of the backlit images.

Fuel Assembly in 35° and 70° Cone Targets

A comparison of the fuel assembly between 35° and 70° cone targets is shown in Fig. 103.7. Backlit images from unfilled 35° [Fig. 103.7(a)] and 70° [Fig. 103.7(b)] targets were recorded using a Fe backlighter. Three images spaced ~ 250 ps apart

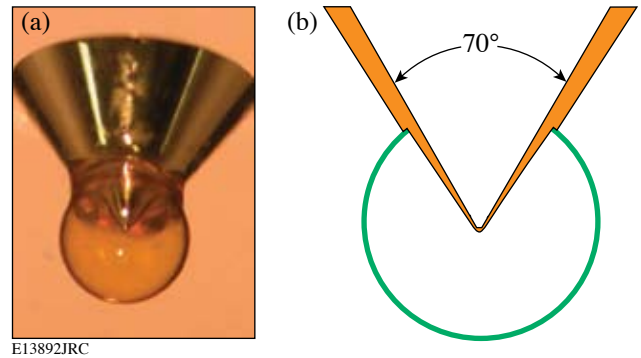


Figure 103.6
Picture of a gas-tight, fast-ignition cone target (a) and a schematic of its cross section (b). A gold cone with an opening angle of 70° is inserted through a hole in a $24\text{-}\mu\text{m}$ -thick CH shell of $\sim 870\text{-}\mu\text{m}$ outer diameter.

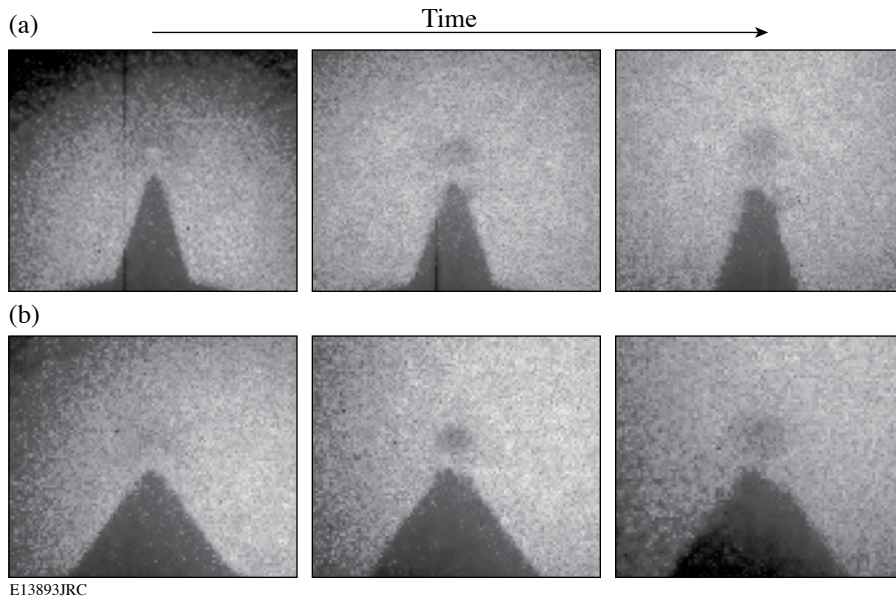


Figure 103.7
Backlit framing camera images from a 35° cone target (a) and a 70° target (b) using a Fe backlighter. Three images spaced ~ 250 ps apart show the assembly of the core and the erosion of the cone, with the central image close to the time of peak compression.

show the assembly of the core, with the central image close to the time of peak compression. The core assembly is similar in both cases, particularly the evolution of the core size. At early times, a horseshoe-shaped dense area is observed, with the opening toward the cone as expected. At peak compression, the core looks quite round and symmetric, with no influence of the cone visible. After peak compression, the core expands in an almost symmetric fashion. Both targets exhaust plasma toward the tip of the cone, eroding the tip at later times. The 35° targets shows less backlighter absorption in the core than the 70° cone targets, possibly due to the incomplete suppression of the core self-emission since the narrow cones are expected to disturb the implosion less and lead to higher core temperatures. The images also show that the plasma flow is directed from the core toward the tip of the cone, an indication that mixing gold and core material is not significant in these implosions.

Mixing of Au Cone and Core Material

Unfilled capsules were used to evaluate the mixing of the gold cone with the CH shell material to compare with previous indirect-drive experiments.¹³ Figure 103.8 shows a backlit image using a V backlighter (a) and a self-emission image (b) taken at the time of peak compression. The backlit image shows absorption outside the original extent of the cone, as indicated by the dashed lines, showing that an expanding plasma is created on the surface of the cone. A gap between the cone tip and core assembly is seen in both images, unlike the data obtained using indirect drive.¹³ The indirect-drive data were interpreted as a 0.04% mass density gold contamination in the compressed shell material. No signatures of mixing were observed in direct drive data; therefore, only an estimate of the minimum detectable gold contamination can be obtained from the analysis of the self-emission images. Figure 103.8(c) shows a lineout through the center of the self-emission image. A Gaussian fit of the core emission shows a symmetric core, with no indication of extra emission because of Au mixing into the core from the cone. At high temperatures (>1 keV) and moderate densities (<1 g/cm³), the plasma conditions expected in the gap, the CH emissivity at 2 to 4 keV is roughly 2,000× smaller than the Au opacity. Consequently, a gold contamination of the order of 0.01% of the mass density in the gap would be visible as an ~10% enhancement of the emission, the estimated error of the symmetry of the emission profile. The x-ray emission from shell plasma in the gap between cone and core reduces the absorption minimum seen in the backlit image. This can be corrected using the self-emission images that show that the emission intensity in the gap is about 1/3 of the emission at the center of the collapsed shell. An analysis of corrected backlit images analogous to the self-emission images using the cold Au

and the hot CH opacities shows no indication of gold plasma streaming into the core with a detection threshold of roughly 0.01% of the mass density.

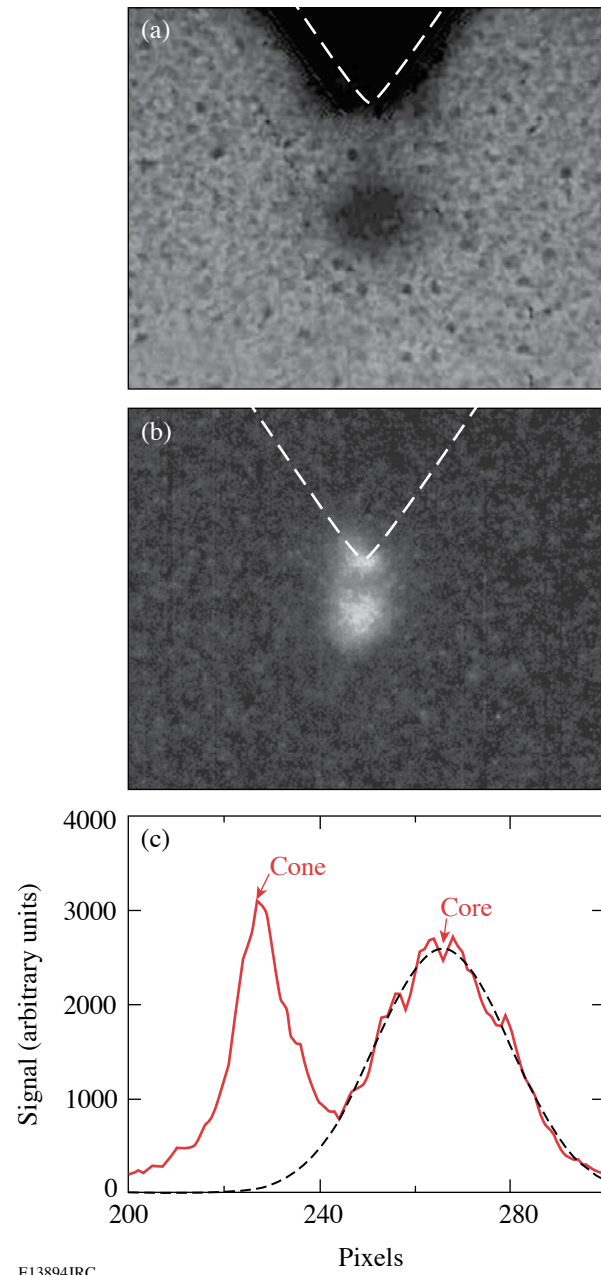


Figure 103.8

(a) Backlit and (b) self-emission x-ray framing camera images of unfilled cone targets obtained using pinhole imaging taken at peak compression. The extent of the cone before the laser shot is indicated with dashed lines. A lineout through the self-emission image is shown in (c).

Compressed Core Areal Density Measurements

The areal density of the assembled core was determined from experiments with targets filled with D^3He gas using nuclear diagnostics. Because of the strong He x-ray emission, the size and location of the hot-fuel region can be inferred from x-ray images of D^3He -filled targets. Figure 103.9(a) shows a backlit x-ray image of a 70° cone target filled with 10-atm D^3He at the time of peak proton production using a Fe backlighter at 6.7 keV. Wedged-range-filter spectrometers²¹ are used to infer the areal density of the compressed shell^{22,23} from the energy loss of the 14.7-MeV primary fusion protons. The proton spectrometers are deployed in two different directions

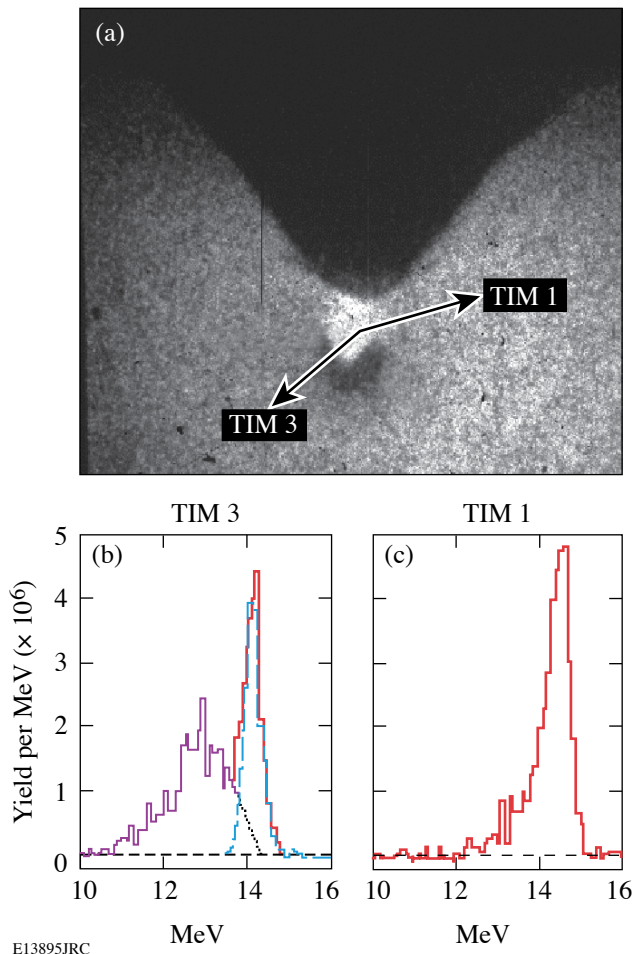


Figure 103.9 Backlit image (a) of a 10-atm, D^3He -filled cone target at time of peak proton production using a Fe backlighter. Significant self-emission from the hot D^3He gas is seen in the image. The directions of the proton spectrometers used to determine the core areal density are indicated as TIM1 and TIM3. D^3He proton spectra taken along two different lines of sight: TIM3 (b) and TIM1 (c).

~15 cm from the target. Figure 103.9(a) shows the line of sight of the two proton spectrometers (labeled TIM1 and TIM3). Figure 103.9 also shows the proton spectra from three 35° cone targets imploded with 55 beams at 21 kJ with a total a proton yield ($\sim 3 \times 10^6$) integrated onto the wedged-range filters in TIM3 (b) and TIM1 (c). Two peaks are observed in the TIM3 spectrum, because the protons detected in TIM3 pass through the dense core (see Fig. 103.9). The narrow peak at ~ 14 MeV is attributed to the shock coalescence phase of the implosion, when the assembled areal density is low.²³ The second, broader peak at ~ 12 MeV is due to protons passing through the dense core close to peak compression.²³ An areal density of $\sim 70 \pm 5$ mg/cm² is inferred from the average energy downshift of ~ 2 MeV (Ref. 21). The protons detected on the TIM2 detector from both the shock and compression phases experience little energy loss and produce only a single narrow peak. The proton yields from the 70° cone targets were about a factor of 2 lower than the yields recorded from the 35° cone targets and showed marginally lower areal densities of $\sim 60 \pm 10$ mg/cm². A fuel ion temperature of 1.2 ± 0.4 keV was inferred from the ratio of the D^3He proton and the DD neutron yields.²²

The experimental areal density values were compared to simulations of full-sphere (no cone) implosions using the 1-D hydrocode *LILAC*.²⁴ *LILAC* predicts a total areal density (shell and fuel) of ~ 90 mg/cm² at the time of peak proton emission for a $24\text{-}\mu\text{m}$ -thick full spherical shell with an average ion temperature of 2.3 keV and a total proton yield of 3×10^8 . The experimental areal density values are more than 66% of the predicted values in both cases. The measured ion temperature is much lower and the measured proton yield is almost three orders of magnitude lower than the simulation yield, showing that the presence of the cone reduces the central hot-spot temperature. Breaking the spherical symmetry by introducing a cone in the shell affects the ion temperature and consequently the proton yield much more than the fuel assembly and the core areal density. Reducing the cone angle from 70° to 35° has a small effect on the areal density. It improves the yield by a factor of 2, though it is still very far from the 1-D predictions.

Cone Filling

The filling of the inside of the cones was investigated using a streaked optical pyrometer (SOP)²⁵ (see Fig. 103.10). The SOP optical system images the inside of the tip of the cone onto the slit of the streak camera with an $\sim 10\text{-}\mu\text{m}$ spatial resolution and a $500\text{-}\mu\text{m}$ field of view. The camera is filtered to record in a wavelength band centered at 660 nm with a 140-nm FWHM to minimize the background from scattered 3ω , 2ω , and 1ω laser light. The breakout of the shock produces a short burst of light.

Its timing relative to peak compression can be determined from the absolute temporal calibration of the SOP with an uncertainty of 50 ps. The shock temperature is inferred from the observed light signal using the absolute calibration of the SOP in intensity with an uncertainty of 10% above ~1 eV (Ref. 26). The number of laser beams used to drive the target is limited to prevent laser light from hitting the inside of the cone and produce a high background signal on the SOP. Figure 103.11(a) shows the SOP streak signal from a 70° cone target irradiated by 48 OMEGA beams with a total energy of ~18 kJ in a 1-ns square pulse. The time axis zero represents the start of the laser pulse. A very clean shock-breakout signal can be seen starting at the tip of the cone and becoming less intense and moving away from the tip as time progresses. Figure 103.11(b) shows a lineout through the center of the SOP trace in comparison with 1-D hydrocode simulations from *LILAC* of the total areal density of the compressed core for a spherical target. The 70° cone targets show a clean shock-breakout signal, similar to data seen in planar shock experiments.²⁷ The shock signal starts well after the time of peak compression (~500 ps) as calculated by *LILAC*, showing that the inside of the cone is free of plasma at the time when the short-pulse laser would propagate. An estimated shock temperature of ~10 eV is obtained using the absolute intensity calibration of SOP.

Conclusions

Fuel-assembly experiments with laser-irradiated, cone-in-shell targets performed on OMEGA indicate that this fast-ignition concept is likely to be scalable to higher energy cryogenic targets. No significant mixing of the gold from the cone with the fuel/shell material was observed, unlike the earlier results seen in the indirect-drive experiments. The core assembly is not severely affected by the presence of the cone, and more than 66% of the expected areal density is inferred from the experiments. Shock-breakout plasma does not begin filling the inside of the cone before peak compression when the ultrafast laser propagates.

In a cryogenic DT ignition capsule, the final core density will be higher, but the core pressure will be similar because of the lower average ionization of the DT compared to CH and the lower-drive adiabat.²⁸ This limits the strength and speed of the shock that causes the inside of the cone to fill with plasma and the erosion of the cone by the core plasma. The thin plastic shell containing the cryogenic fuel radiates much less in cryogenic implosions, reducing the heating and expansion of the gold cone at early times, which minimizes the amount of Au that can mix with the fuel.

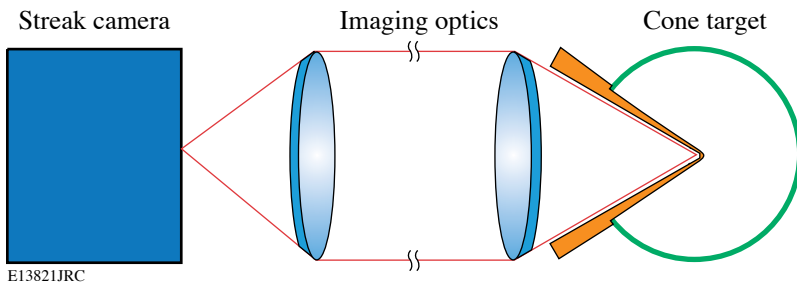


Figure 103.10 Streaked optical pyrometry (SOP) setup used to investigate the filling of the inside of the cone.

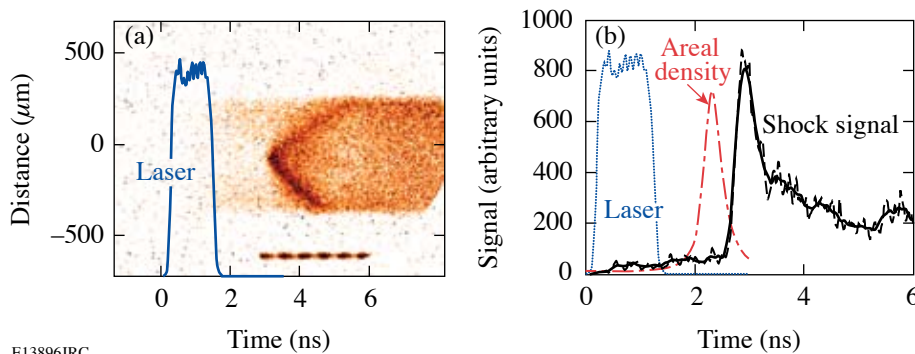


Figure 103.11 Streaked SOP signal from a 70° cone target (a) and lineout through the center of the signal (b) showing a clean shock breakout.

ACKNOWLEDGMENT

The authors are indebted to the Target Fabrication Groups at GA and LLE, especially Mark Bonino, Abbas Nikroo, and Joe Smith. This work was supported by the U.S. Department of Energy Office of Inertial Confinement Fusion under Cooperative Agreement No. DE-FC52-92SF19460, the University of Rochester, and the New York State Energy Research and Development Authority and with corporate support from General Atomics. The support of DOE does not constitute an endorsement by DOE of the views expressed in this article.

REFERENCES

1. N. G. Basov, S. Yu. Gus'kov, and L. P. Feokistov, *J. Sov. Laser Res.* **13**, 396 (1992).
2. M. Tabak *et al.*, *Phys. Plasmas* **1**, 1626 (1994).
3. J. D. Lindl, R. L. McCrory, and E. M. Campbell, *Phys. Today* **45**, 32 (1992).
4. K. Yasuike *et al.*, *Rev. Sci. Instrum.* **72**, 1236 (2001).
5. S. Atzeni, *Phys. Plasmas* **6**, 3316 (1999).
6. Y. T. Li *et al.*, *Phys. Rev. E* **69**, 036405 (2004).
7. R. B. Stephens *et al.*, *Phys. Rev. E* **69**, 066414 (2004).
8. Y. Kitagawa *et al.*, *Phys. Plasmas* **9**, 2202 (2002).
9. M. Tabak *et al.*, Lawrence Livermore National Laboratory Patent Disclosure, IL-8826B, Lawrence Livermore National Laboratory, Livermore, CA (1997).
10. P. A. Norreys *et al.*, *Phys. Plasmas* **7**, 3721 (2000).
11. R. Kodama *et al.*, *Nature* **412**, 798 (2001).
12. R. Kodama *et al.*, *Nature* **418**, 933 (2002).
13. R. B. Stephens *et al.*, *Phys. Rev. Lett.* **91**, 185001 (2003).
14. T. R. Boehly, D. L. Brown, R. S. Craxton, R. L. Keck, J. P. Knauer, J. H. Kelly, T. J. Kessler, S. A. Kumpan, S. J. Loucks, S. A. Letzring, F. J. Marshall, R. L. McCrory, S. F. B. Morse, W. Seka, J. M. Soures, and C. P. Verdon, *Opt. Commun.* **133**, 495 (1997).
15. C. Stoeckl, J. A. Delettrez, J. A. Kelly, T. J. Kessler, B. E. Kruschwitz, S. J. Loucks, R. L. McCrory, D. D. Meyerhofer, D. N. Maywar, S. F. B. Morse, J. Myatt, A. Rigatti, L. J. Waxer, J. D. Zuegel, and R. B. Stephens "High-Energy Petawatt Project at the University of Rochester's Laboratory for Laser Energetics," submitted to *Fusion Science and Technology*.
16. L. J. Waxer, D. N. Maywar, J. H. Kelly, T. J. Kessler, B. E. Kruschwitz, S. J. Loucks, R. L. McCrory, D. D. Meyerhofer, S. F. B. Morse, C. Stoeckl, and J. D. Zuegel, *Opt. Photonics News* **16**, 30 (2005).
17. S. Skupsky and R. S. Craxton, *Phys. Plasmas* **6**, 2157 (1999).
18. T. R. Boehly, V. A. Smalyuk, D. D. Meyerhofer, J. P. Knauer, D. K. Bradley, R. S. Craxton, M. J. Guardalben, S. Skupsky, and T. J. Kessler, *J. Appl. Phys.* **85**, 3444 (1999).
19. Y. Lin, T. J. Kessler, and G. N. Lawrence, *Opt. Lett.* **21**, 1703 (1996).
20. D. K. Bradley *et al.*, *Rev. Sci. Instrum.* **66**, 716 (1995).
21. F. H. Séguin, J. A. Frenje, C. K. Li, D. G. Hicks, S. Kurebayashi, J. R. Rygg, B.-E. Schwartz, R. D. Petrasso, S. Roberts, J. M. Soures, D. D. Meyerhofer, T. C. Sangster, J. P. Knauer, C. Sorce, V. Yu. Glebov, C. Stoeckl, T. W. Phillips, R. J. Leeper, K. Fletcher, and S. Padalino, *Rev. Sci. Instrum.* **74**, 975 (2003).
22. C. K. Li, D. G. Hicks, F. H. Séguin, J. A. Frenje, R. D. Petrasso, J. M. Soures, P. B. Radha, V. Yu. Glebov, C. Stoeckl, D. R. Harding, J. P. Knauer, R. L. Kremens, F. J. Marshall, D. D. Meyerhofer, S. Skupsky, S. Roberts, C. Sorce, T. C. Sangster, T. W. Phillips, M. D. Cable, and R. J. Leeper, *Phys. Plasmas* **7**, 2578 (2000).
23. R. D. Petrasso, J. A. Frenje, C. K. Li, F. H. Séguin, J. R. Rygg, B. E. Schwartz, S. Kurebayashi, P. B. Radha, C. Stoeckl, J. M. Soures, J. Delettrez, V. Yu. Glebov, D. D. Meyerhofer, and T. C. Sangster, *Phys. Rev. Lett.* **90**, 095002 (2003).
24. J. Delettrez, R. Epstein, M. C. Richardson, P. A. Jaanimagi, and B. L. Henke, *Phys. Rev. A, Gen. Phys.* **36**, 3926 (1987).
25. J. A. Oertel *et al.*, *Rev. Sci. Instrum.* **70**, 803 (1999).
26. J. Miller, *Bull. Am. Phys. Soc* **49**, 181 (2004).
27. R. E. Olson *et al.*, *Phys. Rev. Lett.* **91**, 235002 (2003).
28. C. Stoeckl, C. Chiritescu, J. A. Delettrez, R. Epstein, V. Yu. Glebov, D. R. Harding, R. L. Keck, S. J. Loucks, L. D. Lund, R. L. McCrory, P. W. McKenty, F. J. Marshall, D. D. Meyerhofer, S. F. B. Morse, S. P. Regan, P. B. Radha, S. Roberts, T. C. Sangster, W. Seka, S. Skupsky, V. A. Smalyuk, C. Sorce, J. M. Soures, R. P. J. Town, J. A. Frenje, C. K. Li, R. D. Petrasso, F. H. Séguin, K. Fletcher, S. Padalino, C. Freeman, N. Izumi, R. Lerche, and T. W. Phillips, *Phys. Plasmas* **9**, 2195 (2002).
29. T. C. Sangster, J. A. Delettrez, R. Epstein, V. Yu. Glebov, V. N. Goncharov, D. R. Harding, J. P. Knauer, R. L. Keck, J. D. Kilkenny, S. J. Loucks, L. D. Lund, R. L. McCrory, P. W. McKenty, F. J. Marshall, D. D. Meyerhofer, S. F. B. Morse, S. P. Regan, P. B. Radha, S. Roberts, W. Seka, S. Skupsky, V. A. Smalyuk, C. Sorce, J. M. Soures, C. Stoeckl, K. Thorp, J. A. Frenje, C. K. Li, R. D. Petrasso, F. H. Séguin, K. A. Fletcher, S. Padalino, C. Freeman, N. Izumi, J. A. Koch, R. A. Lerche, M. J. Moran, T. W. Phillips, and G. J. Schmid, *Phys. Plasmas* **10**, 1937 (2003).
30. J. A. Delettrez, J. Myatt, P. B. Radha, C. Stoeckl, S. Skupsky, and D. D. Meyerhofer, "Hydrodynamic Simulations of Integrated Experiments Planned for OMEGA/OMEGA EP Laser Systems," submitted to *Plasma Physics and Controlled Fusion*.